Tidal modelling with Thetis: preliminary English Channel benchmarking

Z. Goss[1], S. Warder[1], A. Angeloudis[1], S. C. Kramer[1], A. Avdis[1], and M. D. Piggott*[1]

[1]Department of Earth Science & Engineering, Imperial College London, UK

June 28, 2019

Abstract

This report describes the application and benchmarking of the Thetis coastal ocean model for tidal modelling, and makes use of a test case based upon the English Channel. Comparisons are made between model predictions and tide gauge data at a number of locations across the English Channel. A preliminary investigation of the impact of mesh resolution and bathymetry data is given. A demonstration is also provided of Thetis's ability to use adjoint technology to optimise model predictions through the assimilation of observational data. In the example presented here the bottom friction field is optimised to provide an improved match between the model results and tide gauge data. This adjoint based optimisation capability may also be used to optimise the location, size and design of tidal power generation schemes.

1 Thetis

Thetis[1] is a flexible finite element based coastal ocean model. It is implemented using Python and makes use of the Firedrake[2] system which provides methods for the automatic generation of code for the solution of PDEs from a high level description of the underlying equations. Thetis includes solvers for the depth-averaged nonlinear shallow water equations as well as the three-dimensional hydrostatic [14] and nonhydrostatic [16] equations and associated scalar transport equations. Recent shallow water based applications of the model include simulations of tidal lagoons [1, 12, 17]. The use of array optimisation capabilities to consider competition effects between two tidal turbine arrays built between Alderney and France is described in [11].

The high-level, code generation based design ethos of Thetis, the availability of an adjoint[3] and its use for the purposes of optimising the design of coastal engineering structures, including tidal power generation schemes, is very similar to that developed in the earlier OpenTidalFarm[4] package [9, 10, 5, 6]. However, Thetis possesses a wider range of discretrisation options and the incorporation of more physical processes, including a three-dimensional (3D) baroclinic mode and a wetting and drying capability. Thetis has also been coupled to an optimisation-based anisotropic mesh adaptivity library[5] meaning that it is possible to dynamically update the computational mesh during the course of a simulation in order to improve computational efficiency and/or increase accuracy [15]. Current development activity is implementing goal-based a posteriori error indicators to optimally drive mesh optimisation, is incorporating dispersion effects within the shallow water solver, and coupling to a Lagrangian particle tracking library.

*Corresponding author: m.d.piggott@imperial.ac.uk

[1] http://thetisproject.org/

[2] https://www.firedrakeproject.org/

[3] via the http://pyadjoint.readthedocs.io/ library

[4] http://opentidalfarm.readthedocs.io/

[5] https://github.com/meshadaptation/pragmatic

1.1 Governing equations

The non-conservative form of the nonlinear shallow water equations considered in this work are

$$\frac{\partial \eta}{\partial t} + \nabla \cdot (H_d \mathbf{u}) = 0, \tag{1}$$

$$\frac{\partial \mathbf{u}}{\partial t} + \mathbf{u} \cdot \nabla \mathbf{u} - \nu \nabla^2 \mathbf{u} + f \mathbf{u}^{\perp} + g \nabla \eta = -\frac{\tau_b}{\rho H_d}, \tag{2}$$

where η is the free surface perturbation, H_d is the total water depth and $\mathbf{u} = (u, v)$ is the depth-averaged velocity vector, ν is the kinematic viscosity of the fluid. The term $f\mathbf{u}^{\perp}$ accounts for the Coriolis forcing with $\mathbf{u}^{\perp}$ the velocity vector rotated counter-clockwise 90^o and $f = 2\Omega \sin(\zeta)$, with Ω the angular frequency of the Earth's rotation and ζ the latitude. Due to the size of domain considered in this work a beta-plane approximation to the full Coriolis parameter is employed. Bed shear stress (τ_b) effects are represented here through a Manning's n formulation expressed as:

$$\frac{\tau_b}{\rho} = g n^2 \frac{||\mathbf{u}||\mathbf{u}}{H_d^{\frac{1}{3}}}. \tag{3}$$

1.2 Discretisation

The nature of the underlying Firedrake framework means that Thetis has quite a high level of flexibility over discretisation options. In this work piecewise-linear, discontinuous basis functions are used to represent both velocity and free surface fields (i.e. a so-called $\mathrm{P_{1DG}} - \mathrm{P_{1DG}}$ velocity-pressure finite element pair). A semi-implicit Crank-Nicolson timestepping approach is applied for temporal discretisation with a constant timestep of Δt. Wetting and drying processes are incorporated via the formulation of [13]. Following discretisation, the resulting nonlinear system of equations are solved using a Newton solver from the PETSc[6] library [3].

2 English Channel case study setup

In order to demonstrate the capabilities of Thetis for tidal modelling, we present a case study of the English Channel, validated with tide gauge data. The model is forced at the boundary with Q1, O1, P1, K1, N2, M2, S2 and K2 tidal constituents, except for the optimisation work presented in Section 4 which is forced with only M2. Given the limited extent of the domain under consideration, no astronomical forcing is used in this work. The initial time of the forcing is set to 8am on 6th of May 2003. Simulations are spun up for five days using the function $\tanh(t_{\mathrm{spinup}}/5000)$ where t_{spinup} is a negative time that reaches zero at the end of the spinup period. After the spin-up period the model is run for a full 30 days, with a time step of 100 seconds generally used.

The models all use the wetting and drying scheme from Karna et al (2011) [13], with no minimum depth set and a coefficient of $\alpha = 0.5m$ used in the bathymetry displacement function to ensure positive water depths. For the bottom friction a uniform Manning's n value of 0.023 is used throughout. However, we also present the results obtained using an optimised spatially-varying bed friction field in Section 4.

At open boundaries the free surface evolution is specified using values obtained from OTPS [8], with velocity unconstrained. On all other boundaries no normal flow velocity boundary conditions are imposed.

The horizontal viscosity is set to a value of $\nu = 10$ $\mathrm{m^2 s^{-1}}$ throughout the domain interior; to help with the stability of the model this value linearly ramps up to 1000 $\mathrm{m^2 s^{-1}}$ over a region of size 50km

[6] http://www.mcs.anl.gov/petsc/

from the open boundaries. This 'sponge region' is computed on the mesh during a pre-processing step via the solution to an Eikonal equation which yields distance to boundary information, and which is also implemented as a stand-alone solver withing the Firedrake framework.

In these models high resolution bathymetry from Marine Digimap is used [7] with arc-second resolution ($\approx$ 30 m), however the results if using a GEBCO bathymetry (at 30 arc-second resolution) are also presented.

2.1 Mesh generation

Unstructured triangular meshes are generated for this work using the qmesh package [2]. The model set-up was tested using meshes generated with two sets of shorelines, one highly simplified with the Isle of Wight excluded and the other far more detailed. The former was generated using shorelines from GSHHS[7]. In Section 3.1 we show the results for a mesh with these simplified shorelines, with high resolution with 60,658 elements and using the bathymetry from marine Digimap. In cases where the bottom friction is optimised, in Section 4, we also use this setup.

Since this model employs wetting and drying capabilities, the shorelines of the more detailed mesh are extracted from the Marine Digimap 10m contour, with the smallest estuaries and islands manually excluded using QGIS to avoid excessively complex and large meshes. The model performance is compared for meshes composed of approximately 5690, 19,467 and 72,821 3-node triangles. These meshes have an increased mesh resolution of 2000m, 1000m and 500m at the shorelines and a resolution of 10,000m, 5000m and 2500m over the majority of the domain respectively, all with a gradation distance of 10,000m. The meshes are generated in UTM zone 30 and within this approximately range from a latitude of 341,000 to 832,000 and a longitude of 5,360,000 to 5,640,000 metres.

3 Forward model results

Below we present the results for a variety of different tidal models of the English Channel. They are validated against tide data from 90 gauges situated across the channel sourced from a variety of sources. We present harmonic plots comparing amplitudes from the Thetis simulations and data recorded by the gauges and compare the normalised root mean square error (NRMSE) for different tidal constituents.

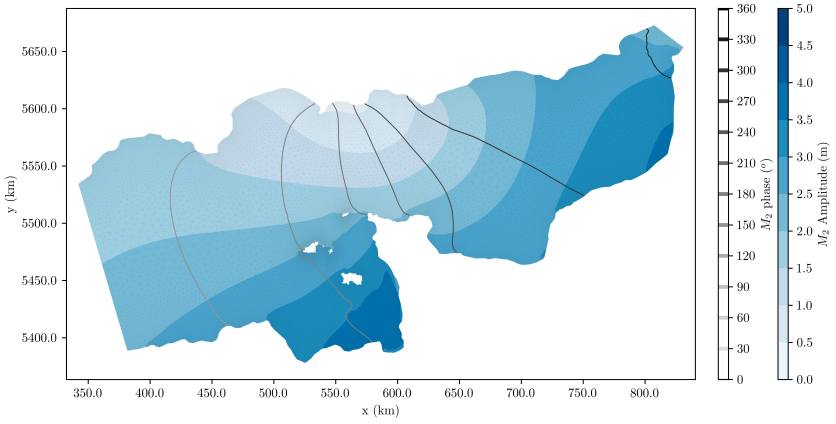

Figure 1: Example of co-tidal chart for M_2 phase and amplitude.

[7] http://www.ngdc.noaa.gov/mgg/shorelines/gshhs.html

3.1 Simplified GSHHS shorelines and high mesh resolution

We have conducted preliminary simulations of the English Channel area over multiple resolutions and levels of coastline detail. Fig. 1 illustrates the spatially varying amplitude and phase of the primary constituent, namely M_2.

Figure 2 presents a scatter plot of the harmonic analysis of the model with simplified GSHHS shorelines, Marine Digimap bathymetry and a relatively fine mesh of 60,658 elements. The results of the Thetis model for the M_2 and S_2 tidal constituents are plotted against that of the tide gauge data. The M2 phase is well predicted with a NRMSE of 0.120 and S2 has a NRMSE of 0.143. This shows the Thetis model set-up is able to produce promising results even for simulations assuming a very simplified coastline representation for the English Channel.

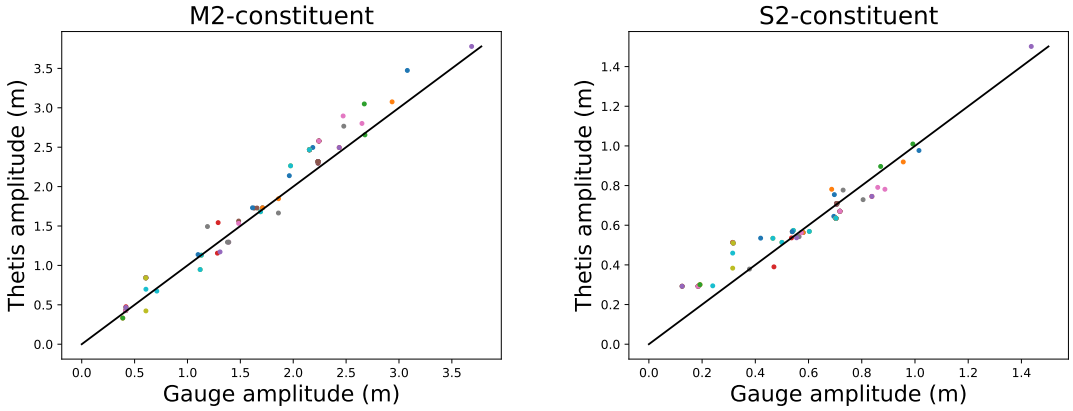

Figure 2: The M2 (left) and S2 (right) harmonic analysis of the models with simplified coastlines, a mesh with 60,658 elements, where the phase found in the thetis model is plotted against that from tide gauges across the English Channel.

3.2 Improved coastlines from Digimap, including the Isle of Wight

Figure 3 shows a snapshot of the instantaneous velocity predicted from the model which uses a Marine Digimap bathymetry and Marine Digimap 10m contour shorelines for a mesh with 19,467 elements. It shows a notably high velocity region in the Alderney Race, which is known to have velocities that exceed 5 ms^{-1} and has an estimated maximum average power potential of 5.1 GW [4].

Figure 4 compares the M2 phase results for models with the same mesh – a very coarse 5,690 element mesh generated using the more detailed Digimap 10m contour shorelines – but comparing use of the Marine Digimap and GEBCO bathymetry. It shows that, counter-intuitively, the results are better when using the GEBCO bathymetry, where we obtain an NRMSE of 0.159 rather than 0.340 using the Marine Digimap bathymetry. It can be seen that even with a very coarse mesh, the model still obtains a reasonable prediction of the M2 constituent.

Likewise, Figure 5 compares the results between Marine Digimap and GEBCO bathymetries, now using a mesh with 19,567 elements. Again a better result is obtained using the GEBCO bathymetry, with an NRMSE of 0.188 compared to 0.392.

These preliminary results, including lack of convergence with mesh resolution, indicate that choice of bathymetry is a key factor in the quality of the results obtained. However, it should be noted that the best results were obtained using the finest mesh, but with a simplified coastline.

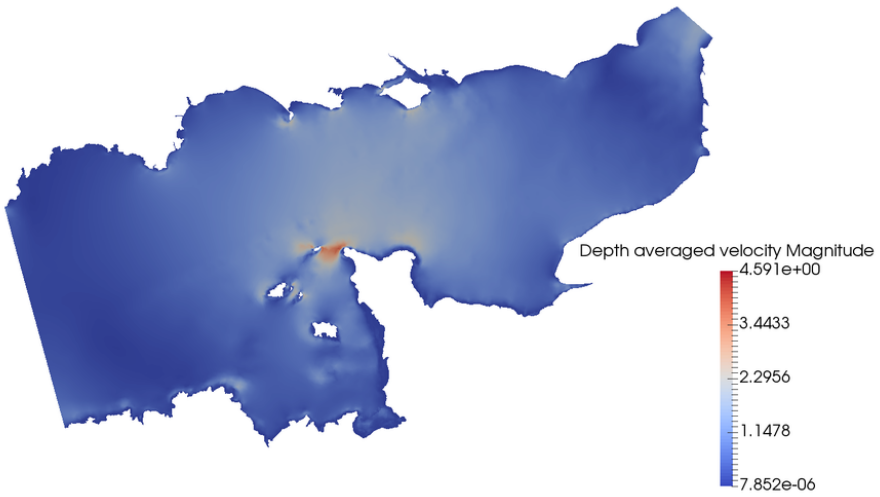

Figure 3: Instantaneous velocity predicted from the Thetis English Channel model, for the Digimap mesh with 19,467 elements.

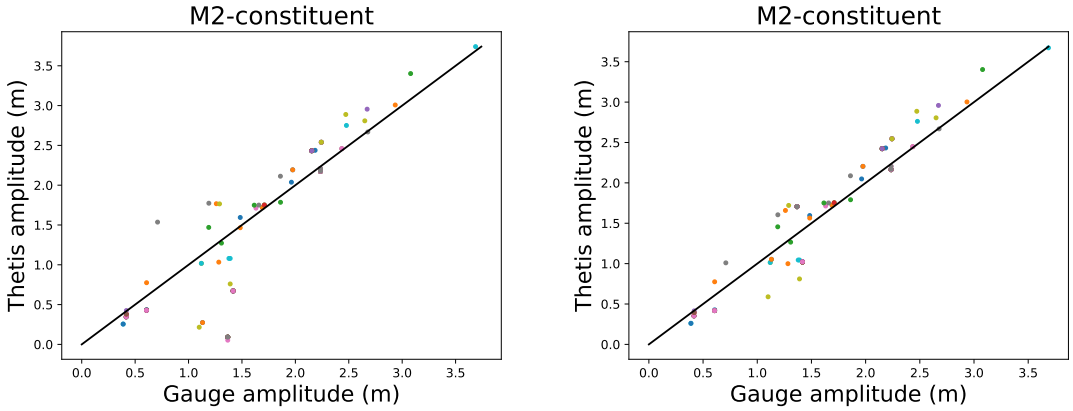

Figure 4: The harmonic analysis of the models with more detailed coastlines, a coarse mesh of 5690 elements, and Marine Digimap (left) or GEBCO (right) bathymetry.

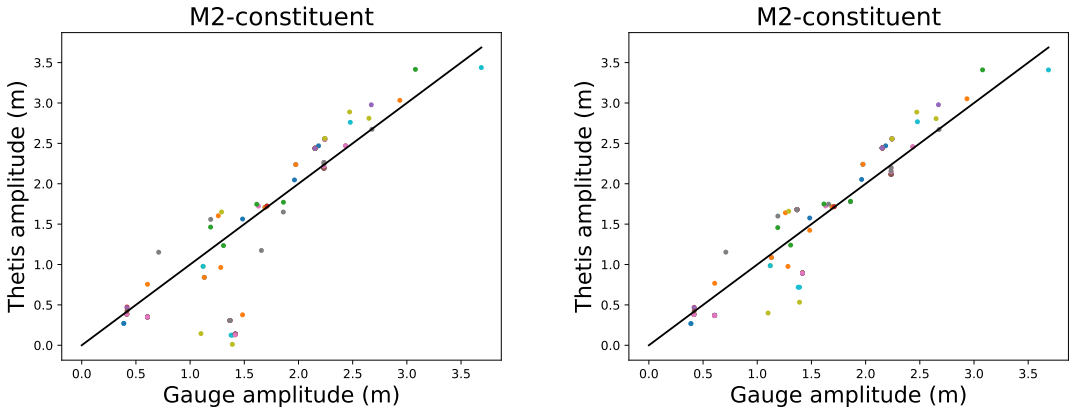

Figure 5: The harmonic analysis of the models with more detailed coastlines, a medium resolution mesh of 19,467 elements and Marine Digimap (left) or GEBCO (right) bathymetry.

4 Optimisation

Tide gauge data within the English Channel was assimilated into the model to generate an improved bottom friction field. Using the adjoint available within Thetis, a gradient-based optimisation method was used to minimise a misfit functional J, defined as

$$J = \sum_i \sum_j \left[\eta_i(t_j) - \hat{\eta}_i(t_j)\right]^2, \tag{4}$$

where η_i is the modelled surface elevation at tide gauge location i, $\hat{\eta}_i$ is the surface elevation at location i generated from tidal harmonics, and j denotes the time step. In order to achieve the minimisation, the value of the Manning bottom drag coefficient was allowed to vary spatially, between limits of 0.005 and 0.1. During each optimisation iteration, the model was run in both forward and adjoint modes, in order to determine the gradient of J with respect to the value of the drag coefficient at each mesh node. The gradient was used to produce updated values of the bottom friction, using the L-BFGS-B optimisation algorithm.

The high-resolution 60,658-element mesh with simplified shorelines was used for the optimisation. The model was forced with only the M2 constituent, for a calibration period of 24 hours. The optimisation was run for 10 iterations, starting with an initial 'guess' for the bottom friction field of 0.023. 32 tide gauge locations were selected for the assimilation; this subset was chosen to achieve an even distribution of gauges over the model domain and avoid any clusters of neighbouring gauges creating a bias in the optimised friction field. Note that, since only a subset of the available tide gauges were used, the results differ slightly from those presented in previous sections.

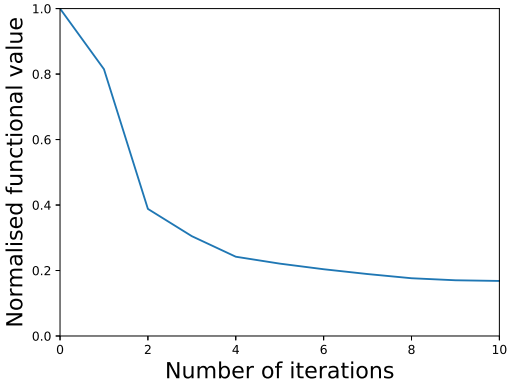

Figure 6: The change in the functional value as the optimisation proceeds. The functional value is substantially reduced during the optimisation.

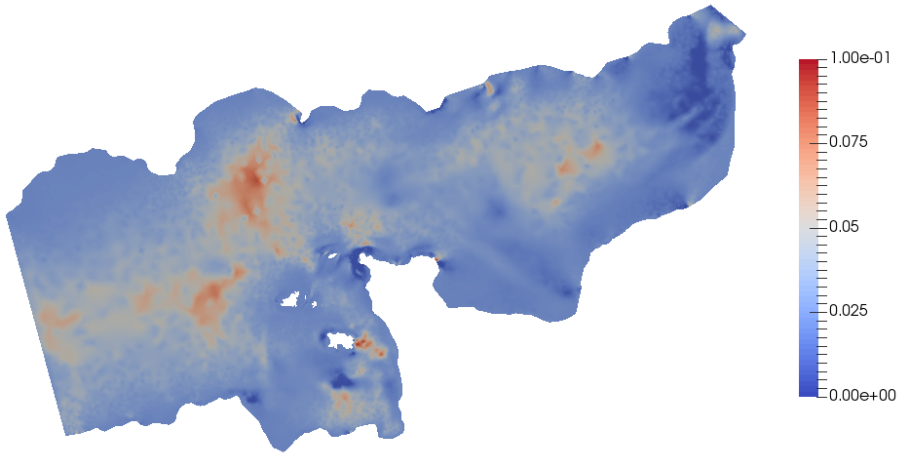

Figure 7: Optimised Manning coefficient field. There are some regions of high friction, but the optimised coefficient value is mostly within a plausible range.

Figure 6 shows the relative decrease of the functional J with each optimisation iteration, and indicates that only a small number of iterations is required to achieve a promising decrease in the functional value. Figure 7 shows the Manning field produced after 10 iterations. While there are regions of high friction, the field mostly takes plausible values.

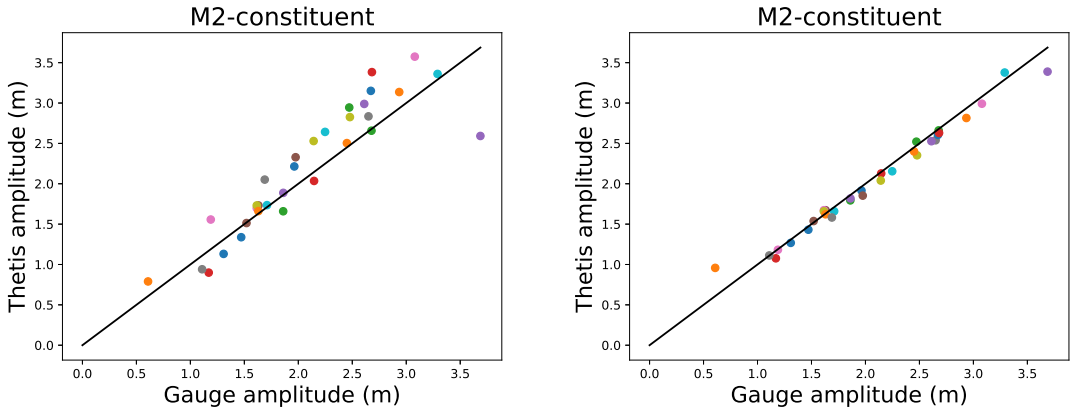

Figure 8: M2 comparison plots (left) using a constant Manning coefficient of 0.023 and (right) using the optimised Manning coefficient field. The NRMSE values are 0.166 and 0.052 respectively.

Figure 8 compares the modelled and predicted M2 amplitudes using the initial and optimised friction fields; the modelled M2 amplitudes are significantly improved as a result of the optimisation, with the NRMSE in M2 amplitude decreasing from 0.166 to 0.052. A plot of the elevation time-series at one of the detector locations is shown in figure 9, showing the improvement to the modelled surface elevation as a result of the optimisation.

5 Conclusions

This preliminary work demonstrates the ability of Thetis to model the tides in the English Channel. The results indicate a complex interplay between resolution of the geometry (the coastlines and the bathymetry), the resolution of the mesh, and parameters such as bed friction. This points to the fact that user-driven calibration of a tidal model is potentially a very challenging undertaking. Section 4 presents a demonstration of how calibration can be automated using optimisaton

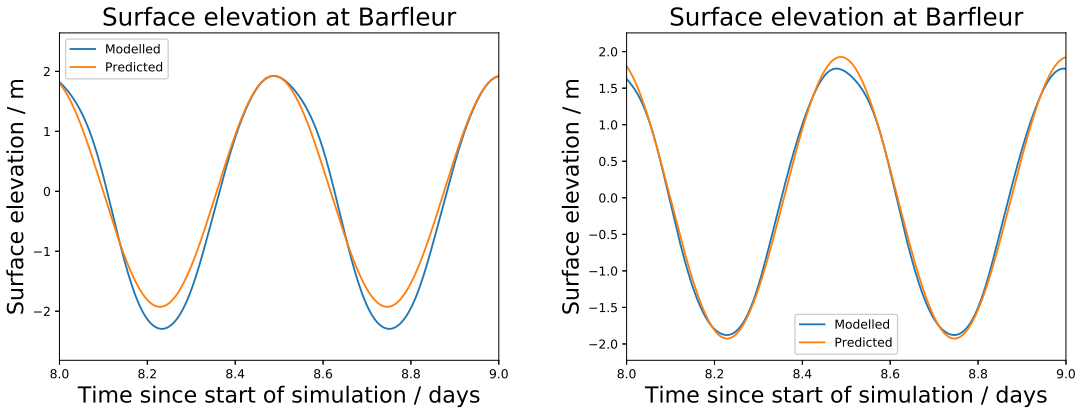

Figure 9: Comparison of the elevation time series at Barfleur, (left) before and (right) after optimisation.

techniques. Here substantially improved model predictions are obtained through the calibration of the bottom friction field. It should be noted that other model inputs can also be optimised in the same manner. However, it should also be noted that improved predictions at the locations where data is assimilated are of course expected; a more thorough analysis should test the overall predictive ability of the model through assimilation of only a subset of the observational data, and then benchmarking of the model at other locations.

References

[1] A. Angeloudis, S. C. Kramer, A. Avdis, and M. D. Piggott. Optimising tidal range power plant operation. *Applied Energy*, 212:680 – 690, 2018.

[2] A. Avdis, A. S. Candy, J. Hill, S. C. Kramer, and M. D. Piggott. Efficient unstructured mesh generation for marine renewable energy applications. *Renewable Energy*, 116:842 – 856, 2018.

[3] S. Balay, S. Abhyankar, M. F. Adams, J. Brown, P. Brune, K. Buschelman, L. Dalcin, V. Eijkhout, W. D. Gropp, D. Kaushik, M. G. Knepley, L. C. McInnes, K. Rupp, B. F. Smith, S. Zampini, and H. Zhang. PETSc users manual. Technical Report ANL-95/11 - Revision 3.7, Argonne National Laboratory, 2016.

[4] D. S. Coles, L. S. Blunden, and A. S. Bahaj. Assessment of the energy extraction potential at tidal sites around the Channel Islands. *Energy*, 2017.

[5] D. M. Culley, S. W. Funke, S. C. Kramer, and M. D. Piggott. Integration of cost modelling within the micro-siting design optimisation of tidal turbine arrays. *Renewable Energy*, 85:215 – 227, 2016.

[6] D. M. Culley, S. W. Funke, S. C. Kramer, and M. D. Piggott. A surrogate-model assisted approach for optimising the size of tidal turbine arrays. *International Journal of Marine Energy*, 19:357 – 373, 2017.

[7] Edina Digimap Service. Hydrospatial one, gridded bathymetry. http://digimap.edina.ac.uk/marine/, 2014. , SeaZone Solutions Ltd, Online; accessed 2017.

[8] G. D. Egbert, S. Y. Erofeeva, and R. D. Ray. Assimilation of altimetry data for nonlinear shallow-water tides: Quarter-diurnal tides of the northwest european shelf. *Continental Shelf Research*, 30(6):668 – 679, 2010. Tides in Marginal Seas - A special issue in memory of Prof Alexei Nekrasov.

[9] S. W. Funke, P. E. Farrell, and M. D. Piggott. Tidal turbine array optimisation using the adjoint approach. *Renewable Energy*, 63:658–673, mar 2014.

[10] S. W. Funke, S. C. Kramer, and M. D. Piggott. Design optimisation and resource assessment for tidal-stream renewable energy farms using a new continuous turbine approach. *Renewable Energy*, 99:1046 – 1061, 2016.

[11] Z. L. Goss, M. D. Piggott, S. C. Kramer, A. Avdis, A. Angeloudis, and C. J. Cotter. Competition effects between nearby tidal turbine arrays—optimal design for Alderney Race. In *Advances in Renewable Energies Offshore: Proceedings of the 3rd International Conference on Renewable Energies Offshore (RENEW 2018), October 8-10, 2018, Lisbon, Portugal*, pages 255–262, 2018.

[12] F. Harcourt, A. Angeloudis, and M. D. Piggott. Utilising the flexible generation potential of tidal range power plants to optimise economic value. *Applied Energy*, 237:873 – 884, 2019.

[13] T. Kärnä, B. de Brye, O. Gourgue, J. Lambrechts, R. Comblen, V. Legat, and E. Deleersnijder. A fully implicit wetting–drying method for DG-FEM shallow water models, with an application to the Scheldt Estuary. *Computer Methods in Applied Mechanics and Engineering*, 200(5):509–524, 2011.

[14] T. Kärnä, S. C. Kramer, L. Mitchell, D. A. Ham, M. D. Piggott, and A. M. Baptista. Thetis coastal ocean model: discontinuous galerkin discretization for the three-dimensional hydrostatic equations. *Geoscientific Model Development*, 11:4359–4382, 2018.

[15] M. Lange M. D. Piggott N. Barral, M. G. Knepley and G. J. Gorman. Anisotropic mesh adaptation in Firedrake with PETSc DMPlex. In *In International Meshing Roundtable*, 2016.

[16] W. Pan, S. C. Kramer, and M. D. Piggott. Multi-layer non-hydrostatic free surface modelling using the discontinuous galerkin method. *Ocean Modelling*, 134:68 – 83, 2019.

[17] C. V. M. Vouriot, A. Angeloudis, S. C. Kramer, and M. D. Piggott. Fate of large-scale vortices in idealized tidal lagoons. *Environmental Fluid Mechanics*, 19(2):329–348, Apr 2019.